

Matching Non-Identical Objects

Yusuke Marumo* Kazuhiko Kawamoto† Hiroshi Kera†‡

Abstract

Not identical but similar objects are everywhere in the world. Examples include four-legged animals such as dogs and cats, cars of different models, akin flowers in various colors, and countless others. In this study, we address a novel task of matching such non-identical objects. We propose a simple weighting scheme of descriptors that enhances various sparse image matching methods, which were originally designed for matching identical objects captured from different perspectives, and achieve semantically robust matching. The experiments show successful matching between non-identical objects in various cases including domain shift. Further, we present a first evaluation of the robustness of the image matching methods under common corruptions, which is a sort of domain shift, and the proposed method improves the matching in this case as well.

1. Introduction

We humans are able to find fine-grained visual correspondences between two objects even when they look similar but not identical or when one is sketched and another appears in a photo. Thanks to this ability, for example, we can identify a cat in a gloomy backstreet from a photo taken in a bright room or assemble components to build a shelf based on its perspective drawing. In computer vision words, this needs fine-grained matching between feature points of two objects under image corruptions, class discrepancy, and domain shift. The classical image matching task [11, 17, 30, 36] only addresses a special case; objects to be matched are assumed to be identical and captured from different perspectives. Recent Transformer-based dense matching methods show great performance on such a matching task [4, 8, 14, 26, 36, 45, 46, 48], and there are also light-weight sparse matching methods, which run in real time with a slight cost in accuracy [3, 11, 19, 23, 27, 30, 44]. However, they do

*Graduate School of Science and Engineering, Chiba University (email: 20t1689w@student.gs.chiba-u.jp)

†Graduate School of Engineering, Chiba University (email: kawa@faculty.chiba-u.jp, kera@chiba-u.jp)

‡Corresponding Author.

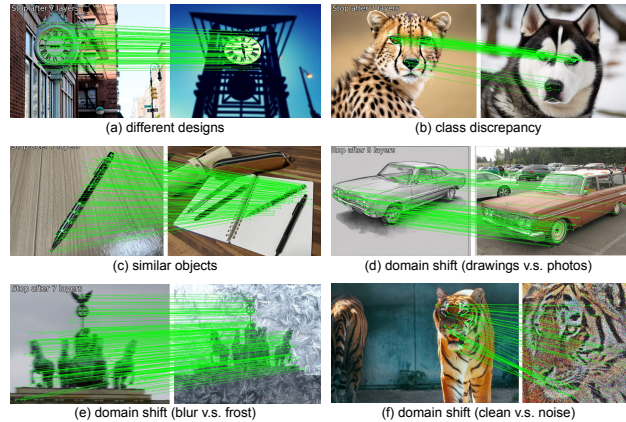


Figure 1. Non-identical object matching is achieved densely and consistently by adding our method between SuperPoint [7] and LightGlue [17]. Object correspondences can be found even when there are (a) design differences, (b) class discrepancy, (c) similar objects, and domain shifts such as (d) drawing v.s. photo and (e,f) different corruptions.

not perform well once the identity assumption is violated and/or objects are captured in harsh environments or different domains (cf. Fig. 2).

In this study, we address a novel task of non-identical object matching, where objects to be matched are not necessarily identical. For example, the objects to be matched can be clocks of different designs or animals of different species. Further, the non-identity naturally induces the necessity of robustness against image corruptions (e.g., blurs and brightness change) and domain shifts (e.g., photo v.s. drawing) because two objects may be captured in different environments and domains, as shown in Fig. 1. A crucial challenge of achieving non-identical object matching is that we cannot simply resort to a supervised learning framework because of the ambiguity of non-identity; there is no ground-truth matching between non-identical objects. At least, to our knowledge, there are no such datasets. Interestingly, we discovered a simple plug-and-play weighting module can extend off-the-shelf sparse matching methods to non-identical object matching. Namely, given a pair of images, sparse matching methods first perform keypoint detection and then feed the extracted descriptors to a feature

matching model to determine the matching of the keypoints. Our weighting module can be inserted before the feature matching model to weight the descriptors using semantic information. Particularly, we introduce an object detector to identify objects and compute a Grad-CAM heatmap [32] to obtain weights. Previously, because of the task definition, matching methods only exploit low-level features, such as colors, edges, and texture, which are all susceptible to ambiguities and perturbations appearing in the non-identical object matching task. The low-level features are still essential to realize fine-grained matching, but the proposed module makes it robust using high-level features.

Our experiments demonstrate that this simple approach significantly boosts the robustness of sparse matching methods, including LightGlue [17] and GlueStick [23], in two tasks: non-identical object matching and robust image matching. In the former task, we evaluate the matching results with various image pairs (a) of the same class, (b) with class discrepancy, (c) with domain shift, and (d) of the same appearance. The sparse matchers alone result in scattered mismatching between non-corresponding areas, but with the addition of our method, fine-grained and consistent matching is achieved. In the latter task, we evaluate the robustness of matching on the MegaDepth-1500 [36] dataset under common corruptions [13] in terms of the AUC score of standard relative pose estimation. The proposed method increases the AUC scores with various types of common corruptions and exceeds a dense matching method LoFTR [36] in the average case.

To summarize, our contributions are as follows:

- We propose non-identical object matching, a novel task of matching similar but unnecessarily identical objects in images even under image corruptions and/or between different domains. This task can be considered a generation of the classical image matching task.
- We propose a simple plug-and-play weighting module that enhances the low-level features using semantic information and successfully extends various sparse matching methods to non-identical object matching.
- We present a first evaluation of the robustness in image matching under common corruptions. By adding corruptions to both input images, the robustness against corruptions itself is measured. By adding them to only one of the input images, the robustness against a domain shift is measured. For both cases, the proposed method is shown useful.

2. Related Work

Image matching [11, 17, 30, 36] is a fundamental task in computer vision with various applications [5, 21, 22, 25, 31, 35, 37, 42] that involves finding the fine-grained correspondence between two images. Many image matching methods consist of two stages. First, a keypoint detector extracts

collections of keypoints, which are pairs of positions and the local feature descriptors. Then, feature matchers find a match between them.

Keypoint detectors. Classically, keypoint detection was done using hand-crafted local features such as SIFT [18] and ORB [29]. Recently, learning-based methods have been developed [7, 10, 12, 40]. Particularly, SuperPoint [7] and DISK [38] are two popular examples. The former is based on convolutional neural networks, and the latter is based on reinforcement learning. There is also a fully differentiable and lightweight method with a minimal model configuration [10]. Unsupervised keypoint detection based on a text-to-image diffusion model [12] also exists. In [40], a flexible technique, which can be combined with other keypoint detectors, is proposed to extract keypoints for robustly performing a matching under illumination changes and repeating texture patterns.

Feature matchers. Feature matchers [43] find a fine-grained correspondence between images. The feature matchers are categorized into two types based on the density of matching points: sparse matchers and dense matchers. The former runs faster, while the latter gives dense and high accuracy. The focus of our study lies in sparse matchers. A seminal sparse matcher, SuperGlue [30], addresses the partial assignment problem for matching by integrating the Transformer attention mechanism [39] with optimal transport [24]. The state-of-the-art sparse matcher, LightGlue [17], improves SuperGlue by introducing a hierarchical matching structure, achieving high matching accuracy and real-time processing simultaneously. GlueStick [23] utilizes line segments for structural features. In contrast to sparse matchers, dense matchers [4, 8, 14, 26, 36, 45, 46, 48] peruse matching accuracy rather than speed. Dense matchers input an image and infer matching using all pixels as keypoints. Therefore, it does not require a keypoint detector so it is also called a detector-free model. LoFTR [36] proposed the first transformer-based method for dense matching, which achieves highly dense matching. Recent studies such as ASpanFormer [4], which controls the attention span, and ASTR [45], which focuses on the role of each pixel.

The aforementioned methods are all designed for image matching and do not perform well in our new task, where objects to be matched do not necessarily appear the same and/or images are corrupted (cf. Fig. 2). There are a few studies that aim at robust matching in particular cases. For example, DarkFeat [11] address matching in low-light conditions, and SAM [19] peruses robustness against large viewpoint change and illumination change. As for such image corruptions, we consider fifteen types of common cor-

ruptions [13], including large brightness change and contrast change.

3. Non-Identical Object Matching

This study introduces non-identical object matching, matching between unnecessarily identical objects in two images. For example, a dog and a cat are not identical but still have similar structures such as two eyes, four legs, and one tail. The same mass-produced products, such as cars of the same model, have the same appearance but are still not identical (e.g., owned by different people). Thus, they can appear in images with largely different backgrounds and lighting conditions.

3.1. Task formulation

In the following, we present a more formal problem setup based on a standard matching pipeline. Note that it is essentially hard to completely formalize the non-identical object matching because of the ambiguity of non-identity, so our formalization is slightly conceptual.

Problem 1 (Non-identical object matching) Let \mathcal{X} be the image domain. Given two images $\mathbf{x}_A, \mathbf{x}_B \in \mathcal{X}$, let $D_A = \{(\mathbf{p}_i^A, \mathbf{d}_i^A)\}_{i=1}^{n_A}$ be n_A keypoints in image \mathbf{x}_A , where $\mathbf{p}_i^A \in \mathbb{R}^2$ and $\mathbf{d}_i^A \in [0, 1]^d$ are the position and the descriptor of i -th keypoint, respectively. We define $D_B = \{(\mathbf{p}_i^B, \mathbf{d}_i^B)\}_{i=1}^{n_B}$ for image \mathbf{x}_B similarly. Let $\mathcal{L}(\cdot)$ be a (conceptual) matching loss function. The non-identical object matching can be formalized as follows.

$$\min \mathcal{L}(\{m_{kl}\}_{k=1, \dots, n_A, l=1, \dots, n_B}) \quad (1)$$

$$\text{s.t. } m_{kl} \in [0, 1], \forall k \in \{1, \dots, n_A\}, l \in \{1, \dots, n_B\} \quad (2)$$

$$\sum_{l=1}^{n_A} m_{kl} \leq 1, \forall k \in \{1, \dots, n_A\} \quad (3)$$

$$\sum_{k=1}^{n_B} m_{kl} \leq 1, \forall l \in \{1, \dots, n_B\}. \quad (4)$$

The matching coefficient $m_{kl} = 1$ indicates that the k -th keypoint in image \mathbf{x}_A and the l -th keypoint in image \mathbf{x}_B is matched and otherwise $m_{kl} = 0$. Each keypoint in one image has at most one matched point in the other image. This condition is implemented by the last two constraints. In the image matching task, where an identical object is captured from different angles in two images, the matching loss $\mathcal{L}(\{m_{kl}\}_{k,l})$ measures the discrepancy between a camera pose computed the matching $\{m_{kl}\}_{k,l}$ and the ground truth.

Our task, non-identical object matching, covers a broader class of matching. Given two images $\mathbf{x}_A, \mathbf{x}_B \in \mathcal{X}$ that contain (potentially non-identical) objects to be matched, image \mathbf{x}_I can be characterized by several attributes (o_I, y_I, P_I, D_I) for $I \in \{A, B\}$. If $o_A = o_B$, then

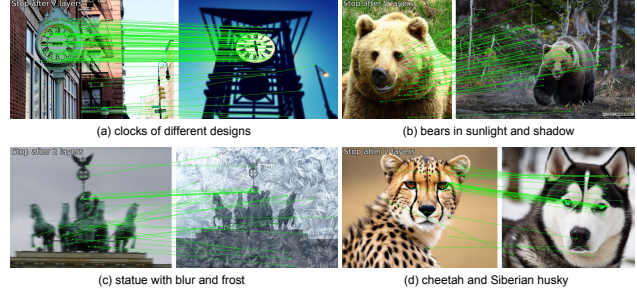


Figure 2. Failure cases of non-identical object matching by SuperPoint [7] as a keypoint detector and LightGlue [17] as the state-of-the-art matcher. (a) The images are matched with backgrounds that have no correspondence. (b) The texture of the bear and the background are matched. (c) The shape of the corruption called frost is matched, because the matcher does not know the existence of the object. (d) There is a large difference in the matches between the right and left eyes. This is because the matcher does not consider the semantics of the object.

the objects to be matched are identical. If $o_A \equiv o_B$, they are the same in appearance but not necessarily identical (e.g., two cars of the same model). If $y_A = y_B$, they belong to the same class (e.g., the car class). If $P_A = P_B$, then they are captured from the same camera pose. If $D_A = D_B$, they are captured in the same domain (e.g., the drawing domain).

The classical image matching corresponds to the case with $o_A = o_B$ (consequently, $o_A \equiv o_B$ and $y_A = y_B$), $P_A \neq P_B$, and $D_A = D_B$. In words, it considers identical objects captured from different camera poses in the same domain. In contrast, non-identical object matching encompasses $y_A \neq y_B$ (consequently, $o_A \neq o_B$ and $o_A \not\equiv o_B$), $P_A \neq P_B$, and $D_A \neq D_B$. Note that we practically assume o_A and o_B to be *similar* in some sense. Below, we highlight two important special cases. For both cases, one may assume $P_A \neq P_B$.

Class discrepancy ($y_A \neq y_B$). Four-legged animals, such as tigers and cats, are objects of different classes but have similar structures. They both have two eyes, four legs, and one tail. We humans can find a part-by-part matching between them, even when there are differences in color, texture, and shape. However, it is not trivial how one can design matching methods to find a fine-grained correspondence while being robust against the difference in details. If such a matching is realized, for example, one may track the running motions of unknown four-legged animals based on those of known ones.

Domain shift ($o_A \equiv o_B, D_A \neq D_B$). We humans can know the flower in the painting on the wall depicts that in the garden. This is a robust fine-grained matching of an identical object in different domains. Typical domain shifts

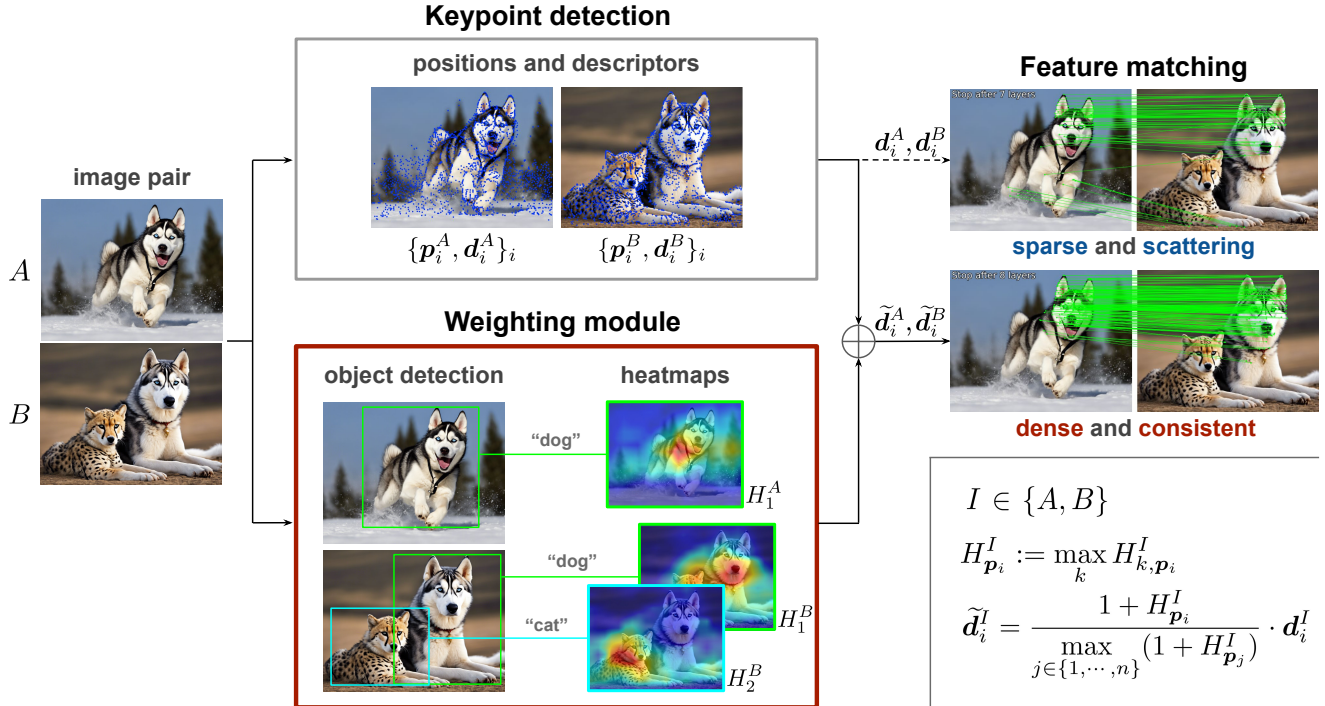


Figure 3. Pipeline of the matching. The keypoint detection and feature matching are done by off-the-self models. The proposed weighting module computes the heatmap scores of objects and weights the descriptors with this semantic information.

include drawings v.s. photos and clean images v.s. corrupted images. For example, suppose that \mathbf{x}_A is a photo and \mathbf{x}_B is a painting. Compared to photos, drawings have fewer colors, textures, and shadows. Thus, while the descriptors of the photo \mathbf{x}_A may reflect the color or texture, those of the drawing \mathbf{x}_B do not, which can lead to an absent of correspondence if the feature matcher is not sufficiently robust. If robust matching between different domains is realized, for example, one can design a system that guides a worker to assemble parts from the first-person video by comparing the parts with those in a blueprint.

3.2. Technical challenges

Generalization from image matching to non-identical object matching introduces ambiguities and perturbations into matching. First, because there is no “correct matching” between two non-identical objects (e.g., a dog and a cat), one cannot resort to a simple supervised learning framework. There is no clear measure of a good matching that can be used for computing a loss to minimize. Second, domain shift by common corruptions or image style significantly changes the low-level features. To our knowledge, existing matching methods only use low-level features such as colors, edges, and textures. As a consequence, these methods are susceptible to the domain shift, as shown in Fig. 2. The first challenge suggests that it would be better to some-

how robustify pretrained image matching models instead of training a model from scratch. The second challenge indicates the necessity of introducing semantic information, which is known to be more robust against domain shifts.

4. Proposed Method

In this section, we present a simple plug-and-play weighting module that can turn various sparse matching models to work for non-identical object matching. Most sparse matching models, such as [3, 17, 23, 30], consist of a pair of a keypoint detector and a feature matcher, and our module process the keypoints before feeding them to the feature matcher. Particularly, given a pair of images $\mathbf{x}_A, \mathbf{x}_B \in \mathcal{X}$, The keypoint detector outputs collections of keypoints $D_A = \{(\mathbf{p}_i^A, \mathbf{d}_i^A)\}_i, D_B = \{(\mathbf{p}_i^B, \mathbf{d}_i^B)\}_i$. The proposed module then computes weighted descriptors $\tilde{\mathbf{d}}_i^A, \tilde{\mathbf{d}}_i^B$ for each $\mathbf{d}_i^A, \mathbf{d}_i^B$, respectively. Lastly, the feature matcher performs matching using $\tilde{D}_A = \{(\mathbf{p}_i^A, \tilde{\mathbf{d}}_i^A)\}_i, \tilde{D}_B = \{(\mathbf{p}_i^B, \tilde{\mathbf{d}}_i^B)\}_i$.

4.1. Weighting module

The proposed weighting module uses an object detector and visual explanation model. In this study, we used YOLOv7 [41] and Grad-CAM [32]. Let $\mathbf{x} \in \mathcal{X}$ be an image, and let $D = \{(\mathbf{p}_i, \mathbf{d}_i)\}_{i=1}^n$ be the collection of n keypoints of \mathbf{x} .

First, the object detector is applied to x and detects the objects with their classes. For each of the detected objects (say, the k -th object), the visual explanation model gives pixel-wise class-activation scores, or a heatmap H_k . Let $H_{k,p_i} \in [0, 1]$ be the heatmap score of H_k at p_i . Then, the heatmap scores at p_i are aggregated as $H_{p_i} := \max_k H_{k,p_i}$. Finally, the weighted descriptor \tilde{d}_i is computed by

$$\tilde{d}_i = \frac{1 + H_{p_i}}{\max_{j \in \{1, \dots, n\}} (1 + H_{p_j})} \cdot d_i \in [0.5, 1]^d. \quad (5)$$

We empirically found that the addition of base value 1 and the normalization by the maximum value is important. For example, the simplest approach $\tilde{d}_i = H_{p_i} d_i \in [0, 1]^d$ ends up with a scarce of matching because of the heatmap scores on the keypoints on background tend to be too low, i.e., $H_{p_i} \approx 0$. Although such keypoints will not likely appear in the matching results, they seem to help the keypoints on objects to be matched. If one instead uses $\tilde{d}_i = (1 + H_{p_i}) d_i \in [1, 2]^d$, this also affects negatively. We consider that this is because of the softmax operations used in the subsequent feature matching. We discuss the consequence of the weighting of descriptors next.

4.2. Effect of weights in feature matcher

We now illustrate how our weighting module affects the subsequent feature matching. We take LightGlue [17] as an example, but a similar discussion holds for other feature matchers. For simplicity, let α_i be the weight in Eq. (5), i.e., $\tilde{d}_i = \alpha_i d_i$. The feature matcher takes as input the keypoints $\tilde{D}_A = \{(p_i^A, \tilde{d}_i^A)\}_i, \tilde{D}_B = \{(p_i^B, \tilde{d}_i^B)\}_i$. The vectors $\tilde{d}_i^A = \alpha_i^A d_i^A, \tilde{d}_i^B = \alpha_i^B d_i^B$ are the i -th weighted descriptors of image x_A, x_B , respectively. Below, symbols with and without $\tilde{\cdot}$ present those with and without weighting.

In the feature matcher, the descriptors are first converted to key and query vectors using matrices $W_q, W_k \in \mathbb{R}^{d \times d}$.

$$\tilde{q}_i^I = W_q \tilde{d}_i^I = \alpha_i W_q d_i^I = \alpha_i q_i^I \quad (6)$$

$$\tilde{k}_i^I = W_k \tilde{d}_i^I = \alpha_i W_k d_i^I = \alpha_i k_i^I, \quad (7)$$

where $I \in \{A, B\}$. Then, the self-attention score a_{ij}^I between i -th and j -th keypoints of image x_I is calculated as follows.¹

$$\tilde{a}_{ij}^I = \tilde{q}_i^{I\top} \mathcal{R}(p_j^I - p_i^I) \tilde{k}_j^I \quad (8)$$

$$= (\alpha_i^I \alpha_j^I) \cdot (q_i^{I\top} \mathcal{R}(p_j^I - p_i^I) k_j^I) \quad (9)$$

$$= (\alpha_i^I \alpha_j^I) \cdot a_{ij}^I. \quad (10)$$

¹To be precise, this score should be considered as the pre-activation score because a softmax operation will be subsequently applied. The terminology of this paper follows the related studies, e.g., [17].

where $\mathcal{R} : \mathbb{R}^2 \rightarrow \mathbb{R}^{d \times d}$ denotes the rotary-encoding [33]. Therefore, our weighting by heatmap scores leads to the weighting of attention scores. The self-attention scores reflect the internal relationship of objects and background, thereby extracting better feature representations in the subsequent steps of the feature matcher. Roughly speaking, nothing that $\alpha_i^I \in [0.5, 1.0]$ for all i and $I \in \{A, B\}$, we have $\alpha_i^I \alpha_j^I \approx 1$ between the keypoints on objects, $\alpha_i^I \alpha_j^I \approx 0.5$ between one on object and the other on background, and $\alpha_i^I \alpha_j^I \approx 0$ for between those on the background. This is reasonable because we want nice feature representations for object keypoints for nice matching. Nevertheless, such nice representations should be obtained by taking into account the background conditions, e.g., to compensate for the overall lighting conditions. If one uses $\alpha_i^I = H_{p_i}$ as discussed earlier, i.e., $H_{p_i} \approx 0$ for background keypoints, the feature representations cannot take into account the background.

Similarly, our weighting affects the cross attention scores. The cross-attention score a_{ij}^{AB} between the i -th keypoint of image x_A and the j -th keypoint of image x_B is computed from the key vectors.

$$\tilde{a}_{ij}^{AB} = \tilde{k}_i^{A\top} \tilde{k}_j^B = (\alpha_i^A \alpha_j^B) \cdot a_{ij}^{AB}. \quad (11)$$

As discussed earlier, the value of $\alpha_i^A \alpha_j^B$ is generally large between the keypoints on objects. Clearly, this encourages the matching between objects.

5. Experiments

We now demonstrate the effectiveness of our method in non-identical object matching tasks. Particularly, we first present qualitative results on various pairs of non-identical (but similar) objects. We then quantitatively evaluate the proposed methods on classical image matching tasks but under common corruptions.

Setup. In the sparse matching framework, the image matching task is performed by a keypoint detector and a feature matcher. For the former, we adopted pre-trained SuperPoint [7], extracting 2,048 keypoints. For the latter, the extracted keypoints are matched using either pre-trained SGMNet [3], GlueStick [23], and the state-of-the-art method, LightGlue [17], with and without the proposed weighting module. We additionally tested a detector-free dense matcher, LoFTR [36]. We downloaded the pretrained models from their official repositories.² All the experiments are conducted on a computer with an NVIDIA GeForce RTX 3090 GPU and 24GB memory.

²SGMNet: <https://github.com/vdvchen/SGMNet>

GlueStick: <https://github.com/cvg/GlueStick>

LightGlue: <https://github.com/cvg/LightGlue>

LoFTR: <https://github.com/zju3dv/LoFTR>

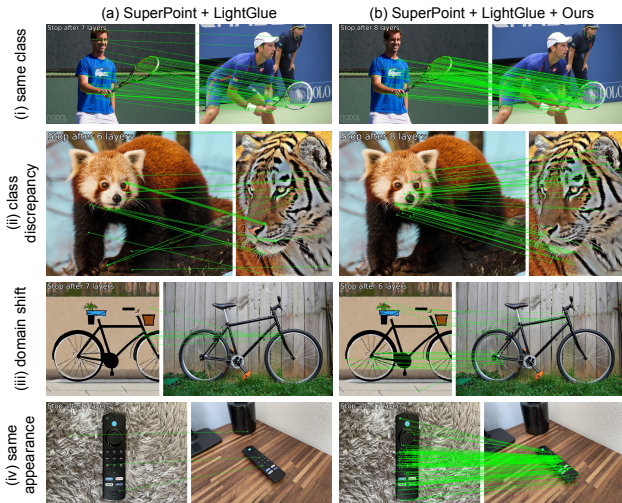


Figure 4. Typical categories of non-identical object matching. (a) A combination of SuperPoint [7] and LightGlue [17] only finds a small number of correspondence, and many of them are incorrect. (b) The proposed method significantly improves the matching.

5.1. Matching Non-Identical Objects

In this experiment, we address a matching of non-identical objects. It is worth noting that this task can only be qualitatively evaluated because there is no ground truth matching between non-identical objects.

Datasets. We collected various images with objects from the COCO [16] and ImageNet [6] datasets. To prepare the drawing version of several images, we used the DreamStudio³, which is backed by the Stable Diffusion [28].

Robust matching across non-identical objects. We examined four cases: (i) same class (i.e., $y_A = y_B, D_A = D_B$), (ii) class discrepancy (i.e., $y_A \neq y_B, D_A = D_B$), (iii) domain shift (i.e., $o_A \equiv o_B, D_A \neq D_B$), and (iv) same appearance (i.e., $o_A = o_B$). For all the cases, we have perspective difference (i.e., $P_A \neq P_B$). Due to the page number restriction, we only present a limited number of matching examples here, but more results can be found in the supplementary material. Figure 4 shows the matching results with and without the proposed method in the four cases. As can be seen in Fig. 4(a), a combination of SuperPoint and LightGlue cannot distinguish between objects and backgrounds or correspond to the same structure of animals. In contrast, Fig. 4(b) shows that the introduction of the proposed method significantly improves the results, reducing unreasonable matchings (e.g., human and racket, animal eye and mouth) and increasing reasonable part-to-part matchings. Particularly, for the cases (i)

³<https://beta.dreamstudio.ai/generate>

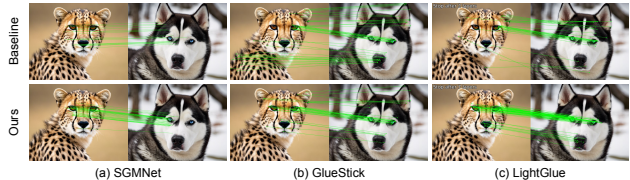


Figure 5. The results with different feature matchers [3, 17, 23]. SuperPoint [7] is used for the keypoint detection. The introduction of the proposed module increases the matching of eyes and noses between the cheetah and Siberian husky and decreases mismatching in the background.

increased the number of matches between rackets and decreased the mismatches between people, (ii) corresponded to the same parts of animals, (iii) matched rear wheels with domain gaps, and (iv) significantly increased the number of matches despite changes in background and object angles. Notably, structural features, such as eyes and noses, are successfully matched between different classes. We consider that the heatmaps of these animals gave similar importance to the eyes or mouth, thus increasing the number of matches between the same parts of the body. In addition, the results for the same class and appearance showed a decrease in mismatches with the background, which means that the background and foreground had relatively lower similarity.

Different matchers. Figure 5 presents the results with different feature matchers, showing that the proposed method boosts all of them to match corresponding parts of the cheetah and Siberian husky.

5.2. Robust Image Matching

We next quantitatively evaluate the proposed method on a standard image matching task but with common corruptions. To our knowledge, we present the first evaluation of the robustness of image matching under common corruptions. We address two cases: (i) both input images are corrupted and (ii) only one of them is corrupted. The former shows the robustness against corruption, and the latter shows the robustness against domain shift (i.e., clean image domain v.s. corrupted image domain).

Dataset. We use image pairs from the MegaDepth-1500 [36] test set as the basis for various experiments. MegaDepth-1500 is a set of 1,500 image pairs from the MegaDepth [15] dataset for two popular phototourism destinations. MegaDepth consists of 3D reconstructed data from one million images, its camera poses and depth maps are first computed from COLMAP [31] and then refined as ground truth. Common Corruptions [13] simulates the 15 types of corruptions that occur when images are captured.

Table 1. The pose accuracy (AUC) at the maximum angular error of 20° of the relative pose estimation from image pairs MegaDepth-1500 [36] under common corruptions. Both images are corrupted with the same type of corruption. The proposed method largely improves LightGlue (LG) [17] and GlueStick (GS) [23] for most categories and the average AUC. The results of a state-of-the-art dense matcher, LoFTR [36], are shown for reference. The proposed method improves the robustness of sparse matchers with a marginal increase in runtime.

Common Corruptions	AUC@ 20° with pairs of corrupted images				
	<i>keypoint detector : SuperPoint</i>				<i>dense</i>
	LG	LG+Ours	GS	GS+Ours	LoFTR
Gaussian Noise	43.09	53.27	45.67	52.24	34.97
Shot Noise	43.41	53.82	46.10	51.72	40.00
Impulse Noise	44.98	50.11	44.91	50.05	37.73
Defocus Blur	32.69	48.35	45.58	49.23	57.22
Frosted Glass Blur	33.37	47.88	47.40	49.94	54.48
Motion Blur	42.12	53.63	44.76	51.84	55.60
Zoom Blur	24.40	31.21	22.87	30.97	23.08
Snow	31.51	30.33	25.26	23.21	31.85
Frost	32.24	31.71	26.39	24.22	19.23
Fog	70.99	73.49	71.19	73.89	67.10
Brightness	75.48	75.08	73.03	70.84	75.45
Contrast	39.50	38.47	39.47	42.61	53.22
Elastic Transform	54.78	66.21	60.37	64.36	58.56
Pixelate	67.94	68.24	65.01	64.81	74.77
JPEG Compression	29.54	36.97	39.66	44.70	59.05
Average	44.40	50.58	46.51	49.64	49.49
Time per pair [msec.]	46.67	68.43	105.72	128.18	312.54

The severity level of corruption is set to 5, which is the most challenging condition.

Metric. We follow the standard evaluation of image matching based on relative pose estimation (e.g., see [17]). From the matching results, the relative pose between two images is computed with RANSAC [9] as follows. First, an essential matrix representing the positional transformation between the images is calculated, which is then decomposed into a rotation and a translation. The camera pose error is computed as the maximum angular error of them, and the area under the cumulative error curve (AUC) at an error of 20° is obtained from it.

Robustness against common corruptions. Table 1 shows the AUC of matching when input images are both corrupted. The results of the dense matching method (i.e., LoFTR) are given for reference. As the results show, the proposed method makes the LightGlue and GlueStick robust against most types of common corruptions (roughly, 5% to 10% increase) with a slight increase in the runtime. The average AUC even exceeds that of LoFTR. The matching methods benefit from the proposed method particularly when images are corrupted by noises and blurs. We ob-

serve AUC decrease in a few types of corruptions, such as Snow and Frost, by the introduction of the proposed method. These corruptions introduce edgy geometric patterns, and the matching methods find correspondence between them. See Section B.1 in the supplementary materials for more detailed comparisons.

Robustness against environmental changes. As the objects to be matched are non-identical, they can appear in largely different environments. Table 2 shows the AUC when only one of the input images is corrupted and the other is clean. As in Tab. 1, the proposed method boosts the LightGlue and GlueStick for most cases and the average case. Interestingly, the results are better for almost all weather categories. For brightness, it is the only one of all categories that shows a decrease in accuracy, but the drop is slight. Weather categories such as Snow and Frost add strong geometry to the overall image, causing mismatches as occlusions. Heatmap weighting is considered to structurally complement the areas hidden by occlusion. The proposed method makes existing matchers robust to environmental changes in general, with a slight precision reduction in clean images. See Section B.2 in the supplementary material for more detailed comparisons.

Table 2. The pose accuracy (AUC) at the maximum angular error of 20° of the relative pose estimation from image pairs MegaDepth-1500 [36] under common corruptions. Only one of the input images is corrupted and the other is a clean image. The proposed method largely improves LightGlue (LG) [17] and GlueStick (GS) [23] for most categories and the average AUC. The results of a state-of-the-art dense matcher, LoFTR [36], are shown for reference. The proposed method improves the robustness of sparse matchers with a marginal decrease in clean accuracy.

Common Corruptions	AUC@ 20° with pairs of clean and corrupted images				
	<i>keypoint detector : SuperPoint</i>				<i>dense</i>
	LG	LG+Ours	GS	GS+Ours	LoFTR
None (Clean)	80.61	78.42	78.04	75.08	80.93
Gaussian Noise	27.54	41.01	41.93	44.98	33.02
Shot Noise	32.10	42.35	41.75	43.82	36.53
Impulse Noise	35.95	43.67	40.97	42.91	34.92
Defocus Blur	18.25	32.13	23.16	30.10	49.40
Frosted Glass Blur	34.25	44.80	42.96	46.21	54.53
Motion Blur	50.07	53.10	44.27	52.69	52.81
Zoom Blur	34.67	40.04	31.18	37.11	31.09
Snow	56.24	58.15	47.22	48.53	49.15
Frost	62.20	64.87	54.34	57.26	43.17
Fog	76.96	78.40	75.18	74.87	74.06
Brightness	77.14	76.98	76.78	75.06	78.41
Contrast	43.09	45.17	40.44	43.53	39.66
Elastic Transform	64.93	68.34	68.02	69.92	68.95
Pixelate	66.80	68.43	67.16	65.46	76.21
JPEG Compression	47.41	53.82	60.39	60.12	68.14
Average	48.51	54.08	50.38	52.84	52.67

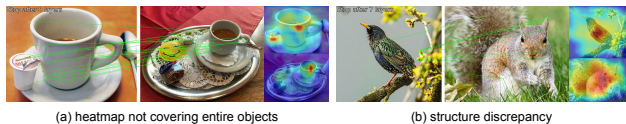


Figure 6. Failure cases. (a) High heatmap scores are given to only a small region of objects to be matched. (b) The structures of objects are clearly different.

5.3. Limitations

We here present failure cases. Figure 6 shows typical cases caused by (a) heatmaps not covering a whole part of objects and (b) great structural differences. In the former case, the importance scores take large only on particular parts of the objects. Further, the large importance scores on the irrelevant object disrupt the matching. This may be resolved by using a better visual explanation model [1, 2, 20, 32, 34, 47]. For the latter case, objects with great structural differences cannot be matched as there is little correspondence between the objects, and eventually, regions of similar colors or textures are matched. To address these cases, one may introduce recent vision and language models to complement the visual information with text features.

6. Conclusion

In this study, we addressed a novel task of non-identical object matching, where objects to be matched are only assumed semantically similar, not necessarily identical as in prior studies. Because of the non-identity, two objects may be captured in different environments and domains. Thus, this task also encompasses robust matching under image corruptions and domain shifts. The proposed method exploits object detection and visual explanation as high-level features, thereby strongly focusing existing feature matchers on objects. Our experiments demonstrated the effectiveness of the proposed method in non-identical object matching and relative pose estimation under various image corruptions.

Acknowledgments

This work was supported by JSPS KAKENHI Grant Number JP22H03658 and JP22K17962. We thank Satomi Tanaka (Ricoh Company, Ltd.) for her fruitful comments and financial support from Ricoh Company, Ltd..

References

- [1] Abnar, S., Zuidema, W.: Quantifying attention flow in transformers. In: Association for Computational Linguistics (2020) [8](#)
- [2] Chattopadhyay, A., Sarkar, A., Howlader, P., Balasubramanian, V.N.: Grad-CAM++: Generalized gradient-based visual explanations for deep convolutional networks. In: Proceedings of the IEEE Winter Conference on Applications of Computer Vision (WACV) (2018) [8](#)
- [3] Chen, Hongkai, Luo, Zixin, Zhang, Jiahui, Zhou, Lei, Bai, Xuyang, Hu, Zeyu, Tai, Chiew-Lan, Quan, Long: Learning to match features with seeded graph matching network. International Conference on Computer Vision (ICCV) (2021) [1](#), [4](#), [5](#), [6](#)
- [4] Chen, H., Luo, Z., Zhou, L., Tian, Y., Zhen, M., Fang, T., Mckinnon, D., Tsin, Y., Quan, L.: ASpanFormer: Detector-free image matching with adaptive span transformer. In: European Conference on Computer Vision (ECCV) (2022) [1](#), [2](#)
- [5] Davison, J., A., Reid, D., I., Molton, D., N., Stasse, Olivier: MonoSLAM: Real-time single camera slam. IEEE Transactions on Pattern Analysis and Machine Intelligence pp. 1052–1067 (2007) [2](#)
- [6] Deng, J., Dong, W., Socher, R., Li, L.J., Li, K., Fei-Fei, L.: ImageNet: A large-scale hierarchical image database. In: Proceedings of the IEEE/CVF Conference on Computer Vision and Pattern Recognition (CVPR). pp. 248–255 (2009) [6](#), [1](#), [2](#), [3](#), [4](#)
- [7] DeTone, D., Malisiewicz, T., Rabinovich, A.: SuperPoint: Self-supervised interest point detection and description. In: Proceedings of the IEEE/CVF Conference on Computer Vision and Pattern Recognition (CVPR) (2018) [1](#), [2](#), [3](#), [5](#), [6](#), [4](#)
- [8] Edstedt, J., Sun, Q., Bökman, G., Wadenbäck, M., Felsberg, M.: RoMa: Robust Dense Feature Matching. arXiv preprint arXiv:2305.15404 (2023) [1](#), [2](#)
- [9] Fischler, M.A., Bolles., R.C.: Random sample consensus: a paradigm for model fitting with applications to image analysis and automated cartography. In: Communications of the ACM (1981) [7](#)
- [10] Gleize, P., Wang, W., Feiszli, M.: SiLK – simple learned keypoints. In: International Conference on Computer Vision (ICCV) (2023) [2](#)
- [11] He, Y., Hu, Y., Zhao, W., Li, J., Liu, Y.J., Han, Y., Wen, J.: DarkFeat: Noise-robust feature detector and descriptor for extremely low-light raw images. In: Association for the Advancement of Artificial Intelligence (AAAI) (2023) [1](#), [2](#)
- [12] Hedlin, Eric, Sharma, Gopal, Mahajan, Shweta, He, Xingzhe, Isack, Hossam, Rhodin, Helge, A.K., Tagliasacchi, Andrea, Yi, Moo, K.: Unsupervised keypoints from pretrained diffusion models. arXiv preprint arXiv:2312.00065 (2023) [2](#)
- [13] Hendrycks, D., Dietterich, T.: Benchmarking neural network robustness to common corruptions and perturbations. In: Proceedings of the International Conference on Learning Representations (ICLR) (2019) [2](#), [3](#), [6](#), [1](#), [4](#)
- [14] Jiang, W., Trulls, E., Hosang, J., Tagliasacchi, A., Yi, K.M.: COTR: Correspondence Transformer for Matching Across Images. In: Proceedings of the IEEE/CVF International Conference on Computer Vision (ICCV) (2021) [1](#), [2](#)
- [15] Li, Z., Snavely, N.: MegaDepth: Learning single-view depth prediction from internet photos. In: Computer Vision and Pattern Recognition (CVPR) (2018) [6](#)
- [16] Lin, T., Maire, M., Belongie, S.J., Bourdev, L.D., Girshick, R.B., Hays, J., Perona, P., Ramanan, D., Dollár, P., Zitnick, C.L.: Microsoft COCO: common objects in context. CoRR (2014) [6](#), [1](#), [2](#), [3](#), [4](#)
- [17] Lindenberger, P., Sarlin, P.E., Pollefeys, M.: LightGlue: Local feature matching at light speed. In: International Conference on Computer Vision (ICCV) (2023) [1](#), [2](#), [3](#), [4](#), [5](#), [6](#), [7](#), [8](#)
- [18] Lowe, D.G.: Distinctive image features from scale-invariant keypoints. In: International Journal of Computer Vision (IJCV) (2004) [2](#)
- [19] Lu, X., Yan, Y., Wei, T., Du, S.: Scene-aware feature matching (2023) [1](#), [2](#)
- [20] Lundberg, M., S., Lee, Su-In: A unified approach to interpreting model predictions. In: Proceedings of the 31st International Conference on Neural Information Processing Systems. p. 4768–4777 (2017) [8](#)
- [21] Moing, G.L., Ponce, J., Schmid, C.: Dense optical tracking: Connecting the dots. arXiv preprint arXiv:2312.00786 (2023) [2](#)
- [22] Mur-Artal, R., Montiel, J.M.M., Tardós, J.D.: ORB-SLAM: A versatile and accurate monocular slam system. In: IEEE Transactions on Robotics (2015) [2](#)
- [23] Pautrat, R., Suárez, I., Yu, Y., Pollefeys, M., Larsson, V.: GlueStick: Robust image matching by sticking points and lines together. In: International Conference on Computer Vision (ICCV) (2023) [1](#), [2](#), [4](#), [5](#), [6](#), [7](#), [8](#)
- [24] Peyré, G., Cuturi, M.: Computational optimal transport. In: Foundations and Trends® in Machine Learning (2019) [2](#)
- [25] Rafi, U., Doering, A., Leibe, B., Gall, J.: Self-supervised keypoint correspondences for multi-person pose estimation and tracking in videos. In: European Conference on Computer Vision (ECCV) (2020) [2](#)
- [26] Rocco, I., Arandjelović, R., Sivic, J.: Efficient neighbourhood consensus networks via submanifold sparse convolutions. In: European Conference on Computer Vision (ECCV) (2020) [1](#), [2](#)

- [27] Roessle, B., Nießner, M.: End2end multi-view feature matching with differentiable pose optimization. In: Proceedings of the IEEE/CVF International Conference on Computer Vision (ICCV) (2023) [1](#)
- [28] Rombach, R., Blattmann, A., Lorenz, D., Esser, P., Ommer, B.: High-resolution image synthesis with latent diffusion models (2021) [6](#), [1](#), [4](#)
- [29] Rublee, E., Rabaud, V., Konolige, K., Bradski, G.: ORB: An efficient alternative to sift or surf. In: International Conference on Computer Vision (ICCV) (2011) [2](#)
- [30] Sarlin, P.E., DeTone, D., Malisiewicz, T., Rabinovich, A.: SuperGlue: Learning feature matching with graph neural networks. In: Proceedings of the IEEE/CVF Conference on Computer Vision and Pattern Recognition (CVPR) (2020) [1](#), [2](#), [4](#)
- [31] Schonberger, J.L., Frahm, J.M.: Structure-from-motion revisited. In: Proceedings of the IEEE/CVF Conference on Computer Vision and Pattern Recognition (CVPR) (2016) [2](#), [6](#)
- [32] Selvaraju, R.R., Cogswell, M., Das, A., Vedantam, R., Parikh, D., Batra, D.: Grad-CAM: Visual explanations from deep networks via gradient-based localization. In: International Conference on Computer Vision (ICCV) (2017) [2](#), [4](#), [8](#)
- [33] Su, J., Lu, Y., Pan, S., Murtadha, A., Wen, B., Liu, Y.: RoFormer: Enhanced transformer with rotary position embedding. In: arXiv preprint arXiv:2104.09864 (2021) [5](#)
- [34] Sumiyasu, K., Kawamoto, K., Kera, H.: Identifying important group of pixels using interactions (2024) [8](#)
- [35] Sun, Jiaming, Wang, Zihao, Zhang, Siyu, He, Xingyi, Zhao, Hongcheng, Zhang, Guofeng, Zhou, Xiaowei: OnePose: One-shot object pose estimation without CAD models. Proceedings of the IEEE/CVF Conference on Computer Vision and Pattern Recognition (CVPR) (2022) [2](#)
- [36] Sun, J., Shen, Z., Wang, Y., Bao, H., Zhou, X.: LoFTR: Detector-free local feature matching with transformers. In: Proceedings of the IEEE/CVF Conference on Computer Vision and Pattern Recognition (CVPR) (2021) [1](#), [2](#), [5](#), [6](#), [7](#), [8](#)
- [37] Sun, J., Wang, Z., Zhang, S., He, X., Zhao, H., Zhang, G., Zhou, X.: OnePose: One-shot object pose estimation without cad models. In: Proceedings of the IEEE/CVF Conference on Computer Vision and Pattern Recognition (CVPR) (2022) [2](#)
- [38] Tyszkiewicz, M.J., Fua, P., Trulls, E.: DISK: Learning local features with policy gradient. In: Neural Information Processing Systems (NeurIPS) (2020) [2](#)
- [39] Vaswani, A., Shazeer, N., Parmar, N., Uszkoreit, J., Jones, L., Gomez, A.N., Kaiser, L., Polosukhin, I.: Attention is all you need. In: Neural Information Processing Systems (NeurIPS) (2017) [2](#)
- [40] Wang, Xinjiang, Liu, Zeyu, Hu, Yu, Xi, Wei, Yu, Wenxian, Zou, Danping: FeatureBooster: Boosting feature descriptors with a lightweight neural network. In: Proceedings of the IEEE/CVF Conference on Computer Vision and Pattern Recognition (CVPR) (2023) [2](#)
- [41] Wang, C.Y., Bochkovskiy, A., Liao, H.Y.M.: YOLOv7: Trainable bag-of-freebies sets new state-of-the-art for real-time object detectors. In: Proceedings of the IEEE/CVF Conference on Computer Vision and Pattern Recognition (CVPR) (2023) [4](#)
- [42] Wang, Q., Chang, Y.Y., Cai, R., Li, Z., Hariharan, B., Holynski, A., Snavely, N.: Tracking everything everywhere all at once. In: International Conference on Computer Vision (ICCV) (2023) [2](#)
- [43] Xu, S., Chen, S., Xu, R., Wang, C., Lu, P., Guo, L.: Local feature matching using deep learning: A survey (2024) [2](#)
- [44] Xue, F., Budvytis, I., Cipolla, R.: IMP: Iterative matching and pose estimation with adaptive pooling. In: Proceedings of the IEEE/CVF Conference on Computer Vision and Pattern Recognition (CVPR) (2023) [1](#)
- [45] Yu, J., Chang, J., He, J., Zhang, T., Wu, F.: Adaptive spot-guided transformer for consistent local feature matching. In: Proceedings of the IEEE/CVF Conference on Computer Vision and Pattern Recognition (CVPR) (2023) [1](#), [2](#)
- [46] Zhang, Y., Zhao, X., Qian, D.: Searching from area to point: A hierarchical framework for semantic-geometric combined feature matching. In: arXiv preprint arXiv:2305.00194 (2023) [1](#), [2](#)
- [47] Zhou, Bolei, Khosla, Aditya, Lapedriza, Agata, Oliva, Aude, Torrallba, Antonio: Learning deep features for discriminative localization. In: Proceedings of the IEEE Conference on Computer Vision and Pattern Recognition. pp. 2921–2929 (2016) [8](#)
- [48] Zhou, Q., Sattler, T., Leal-Taixe, L.: Patch2Pix: Epipolar-guided pixel-level correspondences. In: Proceedings of the IEEE/CVF Conference on Computer Vision and Pattern Recognition (CVPR) (2021) [1](#), [2](#)

Matching Non-Identical Objects

Supplementary Material

A. More matching non-identical objects

In Sec. 5.1 of the main text, we evaluated non-identical object matching by inserting the proposed method between SuperPoint [7] and LightGlue [17]. The matching results for various image pair categories show that the proposed method enhances existing matchers and provides dense and consistent correspondences. To demonstrate this generality for various image pairs, we show more results in three cases: (i) same class (i.e., $y_A = y_B, D_A = D_B$), (ii) class discrepancy (i.e., $y_A \neq y_B, D_A = D_B$), (iii) domain shift (i.e., $o_A \equiv o_B, D_A \neq D_B$).

Setup. We collected various images with objects from the COCO [16] and ImageNet [6] datasets. To prepare drawing or sketch versions of several images, we used the DreamStudio⁴, which is backed by the Stable Diffusion [28]. For details of the experiment, refer to Sec. 5.1.

A.1. Success cases

Figure 7 shows the matching results for the same class case. As in the main text, The introduction of the proposed method turns sparse and inconsistent matching into dense and consistent one. The combination of SuperPoint and LightGlue with our method is robust to object color and shape differences and performs dense and consistent matching. Even in the case of class discrepancy, as shown in Fig. 8, the proposed method successfully corresponds the same parts (e.g., eyes to eyes, nose to nose) between various animals. Figure 9 shows the case of domain shift between images, where our method reduces mismatching caused by image corruptions and image style changes (e.g., photos and drawings). These results indicate that the proposed method can perform accurate matching in many cases under the challenging condition of non-identical object matching.

A.2. Failure cases

There are some cases of failure in non-identical object matching, as shown in Fig. 10. It is difficult to match objects that are of the same class but have significantly different shapes (e.g., the presence or absence of an airplane propeller), or objects that are similar in color or size to other parts (e.g., eyes and nose that are small, round, and black) of the object. Furthermore, image corruptions sometimes hide the texture of the objects, making it difficult to pinpoint the areas to be matched.

⁴<https://beta.dreamstudio.ai/generate>

B. Robust image matching details

With the same setup in Sec. 5.2 of the main text, we evaluate the effectiveness of the proposed method for LightGlue [17] and GlueStick [23] on the robustness to image corruptions and domain shift in image matching. Here, we consider the maximum angular error at 10° and 5° instead of 20°. The results of relative pose estimation with common corruptions [13] on one or both of the input images in the MegaDepth-1500 [36] show that the proposed method improves the robustness of LightGlue and GlueStick.

B.1. Robustness against common corruptions

In this experiment, common corruptions are added to both input images to demonstrate robustness against corruption. Table 3 shows the results of relative pose estimation for maximum angular error of 10° and 5°. As the results show, the proposed method makes the LightGlue and GlueStick robust against most types of common corruptions (roughly, 5% to 10% increase) with a slight decrease in clean accuracy. The average AUC of LightGlue with our method exceeds that of LoFTR [36] in both cases.

B.2. Robustness against environmental changes

In contrast to Sec. B.1, in this experiment, common corruptions are added to one of the image pairs to demonstrate robustness against domain shift between images. Table 4 shows the results of relative pose estimation for maximum angular error of 10° and 5°. As the results show, the proposed method is robust to LightGlue and GlueStick, and in particular, significantly improves the AUC of the former for all Noise, Blur, and Digital categories, and the latter for all Noise and Blur categories. The average AUC of LightGlue with our method exceeds that of LoFTR [36] in both cases.

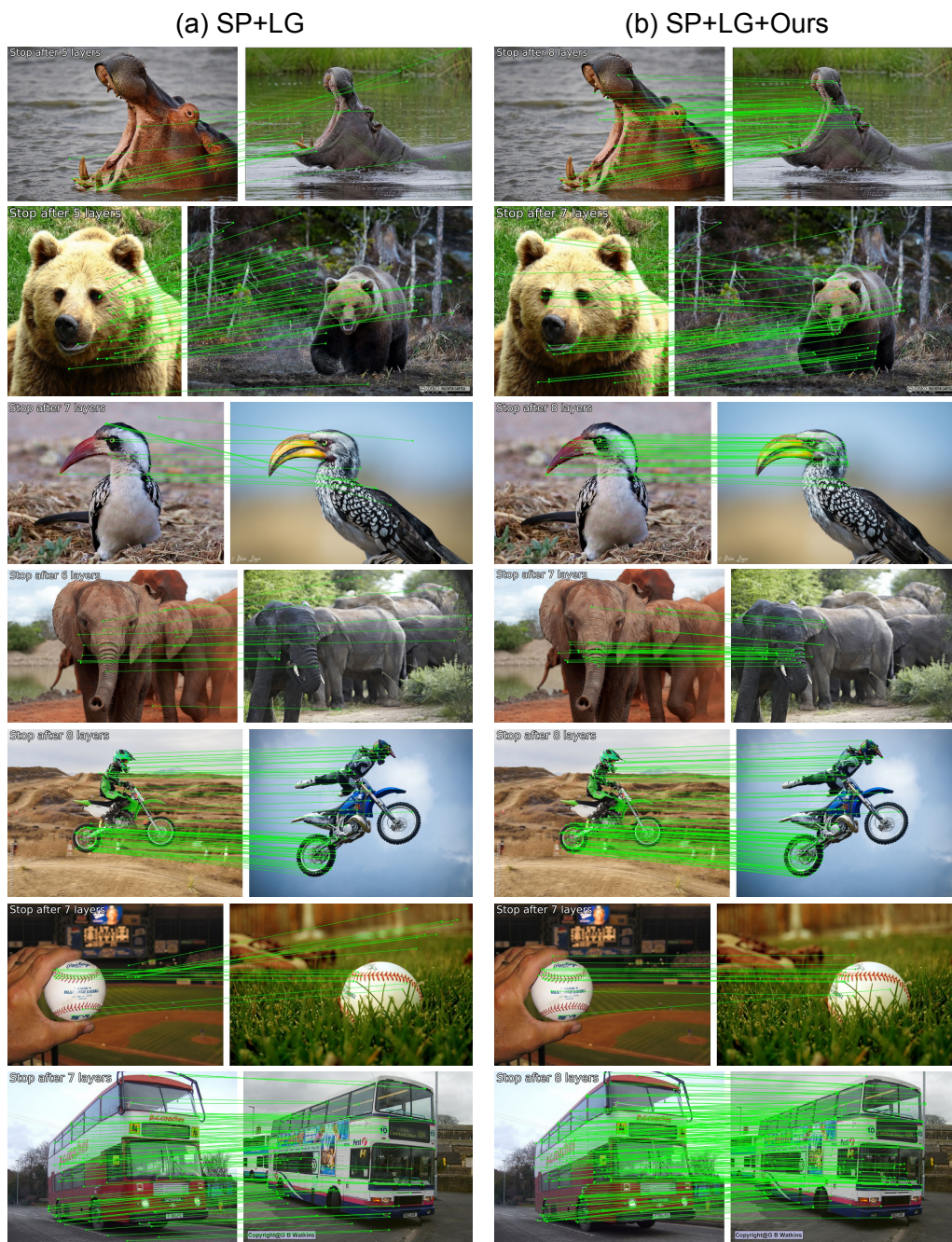


Figure 7. Matching results in the same class case. Image pairs show objects of the same class in ImageNet [6] or COCO [16] datasets. (a) A combination of SuperPoint (SP) [7] and LightGlue (LG) [17] only finds a small number of correspondences, and many of them are incorrect. (b) The proposed method significantly improves the matching and performs dense and consistent correspondences.

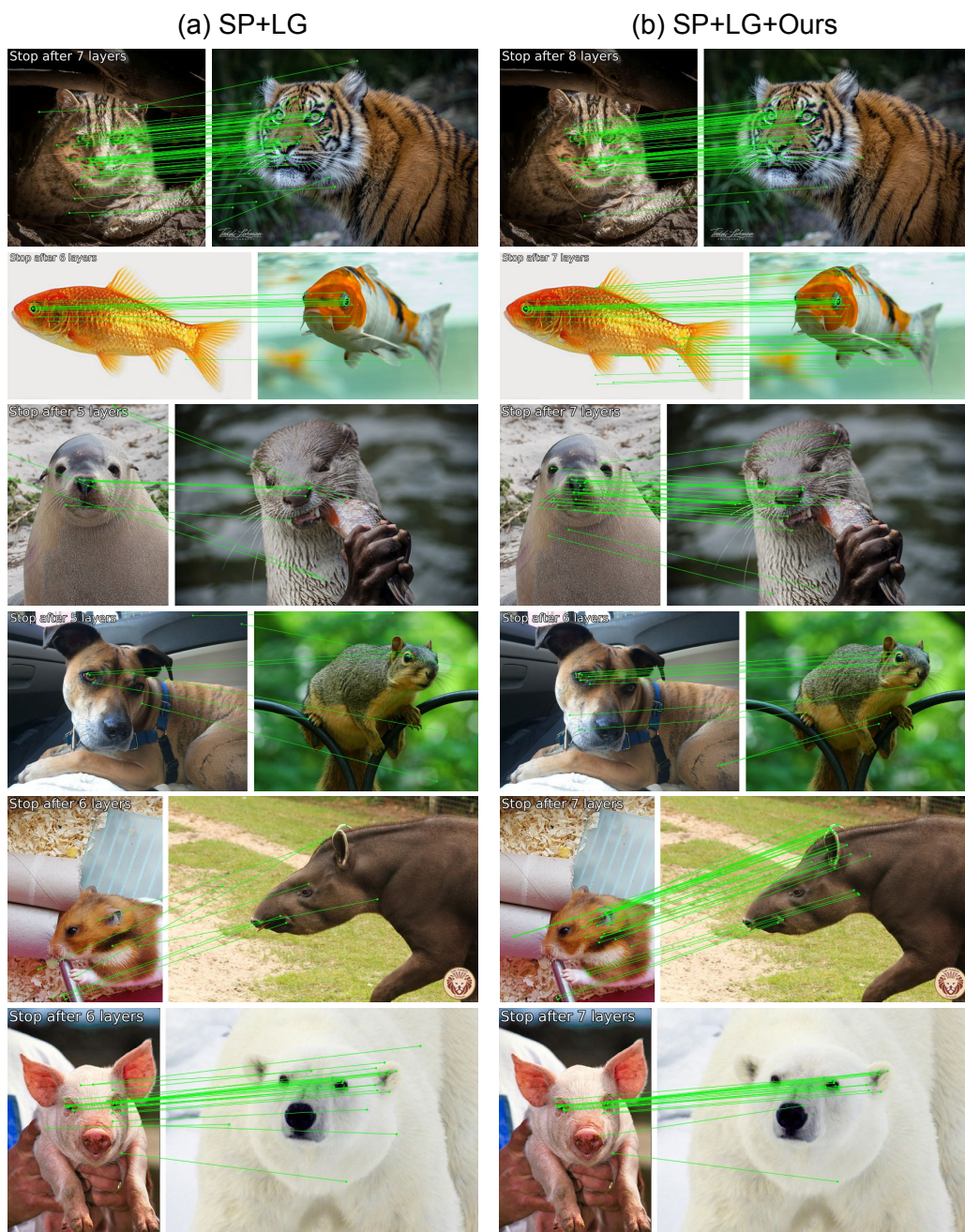


Figure 8. Matching results in the class discrepancy case. Image pairs show objects with class discrepancies in ImageNet [6] or COCO [16] datasets. (a) A combination of SuperPoint (SP) [7] and LightGlue (LG) [17] finds many inconsistent and scattered matches, and it is unclear which is the correct correspondence. (b) The proposed method finds almost all matches for the corresponding parts of the animal, which largely improves the matching to consistency.



Figure 9. Matching results in the domain shift case. Image pairs for matching are ImageNet [6] or COCO [16] datasets with common corruptions [13], and illustrations or sketches of a motorcycle, a violin, and a cat are generated by the Stable Diffusion [28]. (a) A combination of SuperPoint (SP) [7] and LightGlue (LG) [17] finds correct matching, but also finds mismatches with many non-correspondence areas. (b) The proposed method reduces these mismatches and further improves to denser matching between objects.

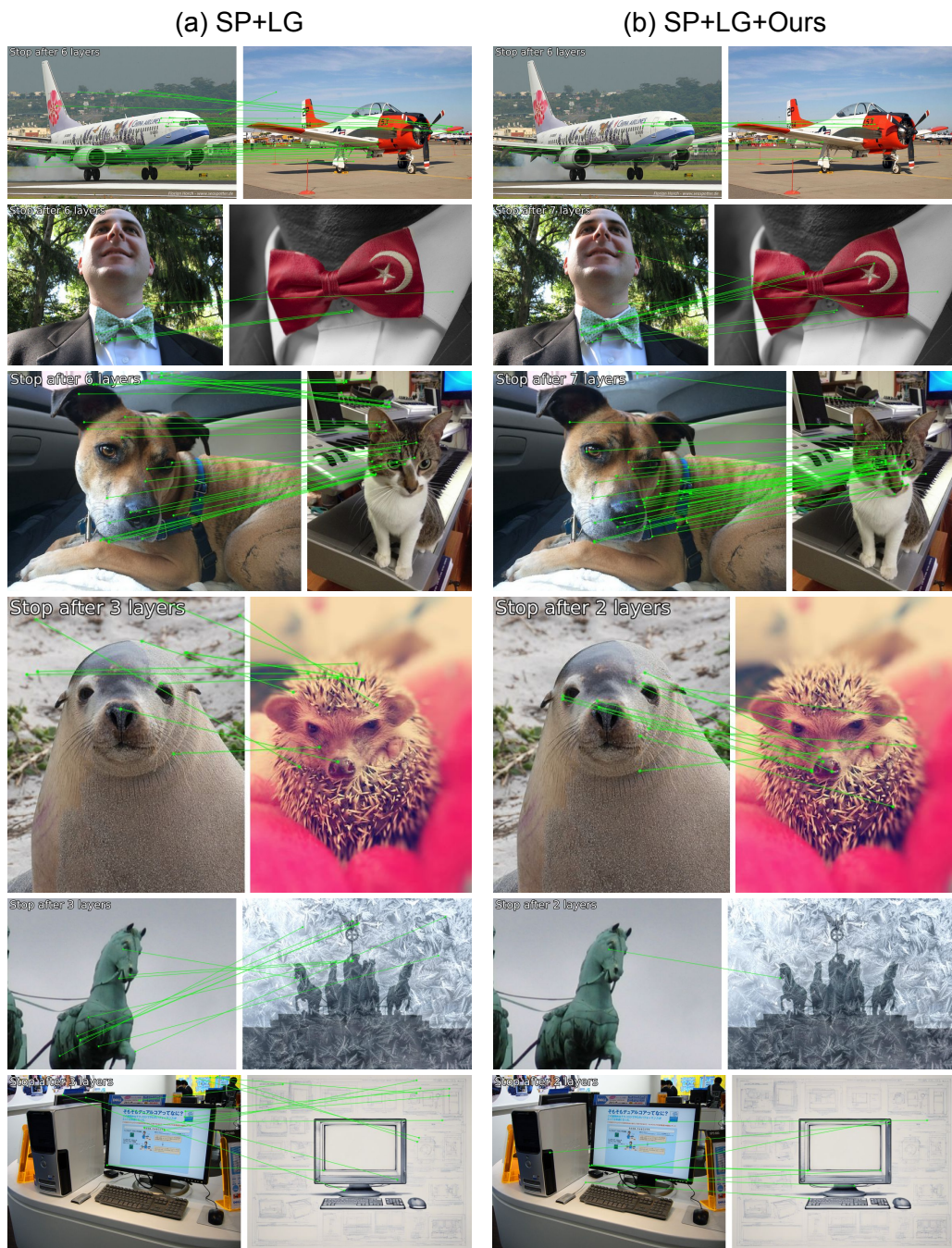


Figure 10. Failure cases of non-identical object matching. (a) A combination of SuperPoint (SP) [7] and LightGlue (LG) [17] fails in matching. (b) The proposed method improves several matchings but still leaves many corresponding areas unmatched.

Table 3. The pose accuracy (AUC) at the maximum angular error of 10° and 5° of the relative pose estimation from image pairs MegaDepth-1500 [36] under common corruptions. Both images are corrupted with the same type of corruption. Our method largely improves LightGlue (LG) [17] and GlueStick (GS) [23] for most categories and the average AUC. The results of a state-of-the-art dense matcher, LoFTR [36], are shown for reference. Our method improves the robustness of sparse matchers with a marginal decrease in clean accuracy.

Common Corruptions	AUC@ 10° with pairs of corrupted images				
	<i>keypoint detector : SuperPoint</i>				<i>dense</i>
	LG	LG+Ours	GS	GS+Ours	LoFTR
None (Clean)	67.89	66.98	64.11	61.94	68.88
Gaussian Noise	27.44	37.28	28.64	35.11	20.07
Shot Noise	27.07	39.79	27.81	33.42	24.27
Impulse Noise	28.70	37.25	29.10	34.44	22.27
Defocus Blur	18.58	24.51	30.12	33.78	43.27
Frosted Glass Blur	17.24	27.61	29.16	31.75	39.21
Motion Blur	27.08	34.85	27.98	35.46	40.68
Zoom Blur	12.50	20.23	12.64	20.72	12.01
Snow	18.35	12.56	12.46	10.49	18.94
Frost	20.86	18.75	17.64	15.48	11.15
Fog	56.32	62.62	55.14	57.24	53.05
Brightness	61.10	63.95	58.75	56.51	61.88
Contrast	24.33	23.10	24.31	27.45	38.57
Elastic Transform	36.76	47.02	41.53	45.52	41.27
Pixelate	51.60	60.66	47.60	47.32	62.55
JPEG Compression	16.60	27.73	22.35	27.64	43.49
Average	29.64	35.86	31.02	34.16	35.51
Common Corruptions	AUC@ 5° with pairs of corrupted images				
	<i>keypoint detector : SuperPoint</i>				<i>dense</i>
	LG	LG+Ours	GS	GS+Ours	LoFTR
None (Clean)	50.43	49.71	45.92	43.11	52.52
Gaussian Noise	14.70	24.44	14.63	21.53	9.85
Shot Noise	13.71	23.44	13.44	18.06	12.21
Impulse Noise	15.65	21.25	16.90	20.64	10.92
Defocus Blur	8.22	11.69	16.59	20.64	27.77
Frosted Glass Blur	7.17	18.09	14.58	16.12	24.59
Motion Blur	14.72	20.72	15.26	22.34	25.37
Zoom Blur	5.38	8.82	6.02	14.16	5.17
Snow	9.48	8.32	5.92	3.87	9.91
Frost	11.92	11.29	9.92	7.72	6.09
Fog	39.01	43.43	35.88	37.58	36.94
Brightness	43.60	47.98	41.86	39.60	45.13
Contrast	11.69	13.93	12.75	15.29	23.13
Elastic Transform	20.43	29.64	24.29	27.28	24.40
Pixelate	32.97	41.82	29.86	29.66	46.40
JPEG Compression	8.00	15.94	9.71	14.79	27.77
Average	17.11	22.72	17.84	20.62	22.38

Table 4. The pose accuracy (AUC) at the maximum angular error of 10° and 5° of the relative pose estimation from image pairs MegaDepth-1500 [36] under common corruptions. Only one of the input images is corrupted and the other is a clean image. Our method largely improves LightGlue (LG) [17] and GlueStick (GS) [23] for most categories and the average AUC. The results of a state-of-the-art dense matcher, LoFTR [36], are shown for reference. Our method improves the robustness of sparse matchers with a marginal decrease in clean accuracy.

Common Corruptions	AUC@10° with pairs of clean and corrupted images				
	<i>keypoint detector : SuperPoint</i>				<i>dense</i>
	LG	LG+Ours	GS	GS+Ours	LoFTR
None (Clean)	67.89	66.98	64.11	61.94	68.88
Gaussian Noise	16.63	28.34	28.57	32.42	24.17
Shot Noise	19.97	32.50	26.23	29.92	26.58
Impulse Noise	23.56	34.74	33.12	36.26	25.67
Defocus Blur	8.29	22.43	12.03	18.17	36.85
Frosted Glass Blur	19.00	32.78	26.39	29.66	40.40
Motion Blur	33.29	39.69	27.88	38.30	39.41
Zoom Blur	20.38	26.23	16.76	25.67	21.60
Snow	39.74	41.07	30.74	33.00	35.91
Frost	47.61	51.78	38.80	41.62	32.97
Fog	62.39	64.08	61.11	60.80	60.74
Brightness	63.40	61.75	62.69	60.04	65.64
Contrast	27.81	33.12	25.86	28.95	30.27
Elastic Transform	47.62	56.66	52.17	55.08	53.61
Pixelate	50.14	56.68	50.33	48.63	63.14
JPEG Compression	29.92	40.31	40.93	40.61	53.58
Average	33.98	41.48	35.57	38.61	40.70
AUC@5° with pairs of clean and corrupted images					
None (Clean)	50.43	49.71	45.92	43.11	52.52
Gaussian Noise	8.42	20.10	16.51	20.52	16.68
Shot Noise	10.30	20.52	16.14	19.31	18.14
Impulse Noise	12.88	24.11	21.41	25.35	17.75
Defocus Blur	3.22	17.92	5.95	15.89	24.73
Frosted Glass Blur	8.56	22.42	15.54	18.79	26.87
Motion Blur	18.95	26.22	13.94	24.36	25.92
Zoom Blur	9.81	19.27	8.95	17.68	15.03
Snow	22.94	26.90	17.27	20.56	23.94
Frost	31.58	37.80	24.13	27.95	23.07
Fog	44.49	45.00	42.65	41.24	44.04
Brightness	46.14	45.24	43.91	41.63	48.85
Contrast	14.98	17.15	14.46	17.53	21.09
Elastic Transform	29.34	39.29	32.27	35.11	36.41
Pixelate	31.51	38.02	31.82	30.10	46.26
JPEG Compression	15.86	27.55	22.24	21.87	37.35
Average	20.60	28.50	21.81	25.19	28.41